

Microscopic analysis of prolate-oblate shape phase transition and shape coexistence in the Er-Pt region

X. Q. Yang,¹ L. J. Wang,¹ J. Xiang,^{2,*} X. Y. Wu,³ and Z. P. Li^{1,†}

¹School of Physical Science and Technology, Southwest University, Chongqing 400715, China

²School of Physics and Electronic, Qiannan Normal University for Nationalities, Duyun 558000, China

³College of Physics and Communication Electronics, Jiangxi Normal University, Nanchang 330022, China



(Received 3 December 2020; revised 15 April 2021; accepted 7 May 2021; published 24 May 2021)

The shape transition and possible occurrence of low-energy shape coexistence and rigid triaxial deformation are analyzed in the six even-even Er, Yb, Hf, W, Os, and Pt isotopic chains with the neutron number $102 \leq N \leq 124$, using a five-dimensional collective Hamiltonian (5DCH) based on covariant density-functional theory. The potential-energy surfaces display a transition from prolate to oblate or triaxial, and then to near spherical shapes as the neutron number increases. The corresponding 5DCH model calculations reproduce the empirical isotopic trend of the characteristic collective observables and confirm the overall shape transition in this region. It is emphasized that a rapid shape transition between prolate and oblate shapes is predicted in Er and Yb isotopic chains while it becomes smooth for higher-Z isotopic chains and signature for rigid triaxial deformation is found in the transitional isotopes, e.g., ^{194}W and $^{192-196}\text{Os}$ by analyzing the energy staggering and probability density distribution in the γ bands. Finally, the calculated low-lying spectra for ^{184}Er and ^{186}Yb demonstrate a remarkable multishape coexistence of medium-deformed oblate, medium- and large-deformed prolate shapes in both nuclei.

DOI: [10.1103/PhysRevC.103.054321](https://doi.org/10.1103/PhysRevC.103.054321)

I. INTRODUCTION

The study of shapes, their evolution and transitions, provides crucial information on the origin of nuclear collectivity and modification of shell structures in nuclei far from stability [1,2]. As the number of nucleons changes from nucleus to nucleus, in general one observes a gradual evolution of different shapes—spherical, axially deformed, γ -soft. An especially interesting feature is the possible occurrence of shape phase transitions (SPTs) for particular values of the number of protons and neutrons. Typical examples are the first-order spherical-to-axially deformed [3] and the second-order spherical-to- γ -soft [4] SPTs. Other types of transitions include the one that occurs between prolate and oblate configurations going through a transitional γ -soft shape [5]. Over the past decades, numerous experimental and theoretical studies of nuclear SPTs have been done [6–8].

A particularly interesting region of the chart, where prolate, oblate, γ -soft or rigid, and spherical shapes are observed and predicted is the tungsten-osmium-platinum region with $A \approx 180$ –200. A prolate-to-oblate SPT is predicted to appear when moving towards the $N = 126$ shell closure. These facts make the region a potential testing ground to understand the deformation properties and underlying shell structures of atomic nuclei. As a result, this region has attracted much experimental and theoretical effort in recent years. Experimental endeavor has mainly focused on spectroscopy to characterize the shape of the low-lying excited states [9–24]. Generally

speaking, the measurements reveal the trend of shape evolution, namely from prolate to oblate then to spherical shapes passing through a γ -unstable or triaxial rotor as the neutron number increases. However, for a better understanding of nuclear-structure evolution in this region it is important to have a more complete picture of absolute transition strengths, which are missing from or disagreeing with experiments using different methods. Theoretical calculations have also been carried out within several frameworks [21–38]. In the past four decades, the mean-field approach with a variety of interactions has been widely used to calculate the potential-energy surfaces and investigate the corresponding shape evolution. The results suggest a sharper transition from axially deformed prolate to axially deformed oblate in the lower-Z (Yb, Hf) nuclei than in the higher-Z isotopic chains, which are predicted to become increasingly γ -soft or have triaxial ground states. Recently, state-of-the-art beyond-mean-field approaches, such as generator coordinate method (GCM) [22,23] and interacting boson mapping method [31,32], based on energy density functionals have been applied to study the collective characters of the low-lying states in this region and demonstrated the prolate-to-oblate SPT.

Nuclear shape phase transitions are, in many cases, accompanied by shape coexistence (SC), which is the coexistence of a sets of nearly degenerate low-energy states characterized by different geometrical shapes in a single nucleus [1]. A typical example is shape transition in the neutron-rich Sr and Zr isotopes around $N = 60$, where coexistence of spherical and large prolate shapes is confirmed in the transitional nuclei $^{96,98}\text{Sr}$ [39–41] and ^{98}Zr [42,43]. Therefore, it is interesting to check whether possible SC appears in the region with $Z < 80$, where prolate-to-oblate SPT is predicted, especially

*jxiang@sgmtu.edu.cn

†zpliphy@swu.edu.cn

when considering the fact that SC is widely reported in the neutron-deficient Pb and Hg isotopes [1]. Another interesting question is how about the softness of triaxial deformation in the transitional nuclei in this region, in particular, whether nuclei can exhibit rigid triaxiality in their low-lying structure. To this end, a fully systematic and microscopic study of the shape evolution in this region, especially including the measurable signatures to characterize the triaxiality, shape phase transition, and coexistence, is necessary.

The covariant density-functional theory (CDFT) [44–47] embeds the fundamental Lorentz invariance from the very beginning and naturally includes the spin-orbit interaction [48–51], which proves to be a successful theory used over the whole nuclide chart, from relatively light systems to superheavy nuclei [46,52–55], from the valley of β stability to the drip lines [46,56–59], and from collective rotations to collective vibrations [60–67]. To take into account the beyond-mean-field effects and describe the low-lying excited states, in the past decade, the five-dimensional collective Hamiltonian based on CDFT (5DCH-CDFT) has been developed [68–70] and achieved great success in the studies of shape phase transitions [68–74], shape coexistence [75–79], and nuclear triaxiality [80,81]. In the present work we will apply 5DCH-CDFT to perform a systematic analysis of the shape evolution, including both potential-energy surfaces (PESs) and measurable collective observables deduced from low-lying spectra, in the six even-even Er, Yb, Hf, W, Os, and Pt isotopic chains with $102 \leq N \leq 124$. Here, in addition to the three higher-Z isotopes, we also consider the three lower-Z neutron-rich Er, Yb, and Hf isotopes, which could be explored in future experiments in facilities for rare-isotope beams [82,83].

In Sec. II we present a short outline of the theoretical framework for 5DCH-CDFT. The systematics of PESs, the evolution of characteristic collective observables, and the energy staggering in the γ band in even-even Er-Pt isotopes are discussed in Sec. III. Section IV summarizes the principal results.

II. THE FIVE-DIMENSIONAL COLLECTIVE HAMILTONIAN

Nuclear energy-density-functional-based studies of low-energy structure phenomena start from a self-consistent mean-field (SCMF) calculation of deformation-energy surfaces with mass multipole moments as constrained quantities. The static nuclear mean-field is characterized by the breaking of symmetries of the underlying Hamiltonian—translational, rotational, and particle number and, therefore, includes static correlations, e.g., deformations and pairing. To calculate excitation spectra and electromagnetic transition rates it is necessary to extend the SCMF scheme to include collective correlations that arise from symmetry restoration and fluctuations around the mean-field minima.

Low-energy excitation spectra and transitions can be described by using a collective Hamiltonian, with deformation-dependent parameters determined from microscopic SCMF calculations. For instance, in the case of quadrupole degrees of freedom, excitations determined by quadrupole vibrational

and rotational degrees of freedom can be described by considering two quadrupole collective coordinates β , γ and three Euler angles $\Omega \equiv (\phi, \theta, \psi)$ [68]. The corresponding 5DCH Hamiltonian takes the following form:

$$\hat{H}(\beta, \gamma, \Omega) = \hat{T}_{\text{vib}} + \hat{T}_{\text{rot}} + V_{\text{coll}}, \quad (1)$$

where V_{coll} is the collective potential that includes zero-point energy (ZPE) corrections, and \hat{T}_{vib} and \hat{T}_{rot} are the vibrational and rotational kinetic-energy terms, respectively [68,84,85],

$$\begin{aligned} \hat{T}_{\text{vib}} = & -\frac{\hbar^2}{2\sqrt{wr}} \left\{ \frac{1}{\beta^4} \left[\frac{\partial}{\partial \beta} \sqrt{\frac{r}{w}} \beta^4 B_{\gamma\gamma} \frac{\partial}{\partial \beta} \right. \right. \\ & - \frac{\partial}{\partial \beta} \sqrt{\frac{r}{w}} \beta^3 B_{\beta\gamma} \frac{\partial}{\partial \gamma} \Big] + \frac{1}{\beta \sin 3\gamma} \left[-\frac{\partial}{\partial \gamma} \right. \\ & \times \sqrt{\frac{r}{w}} \sin 3\gamma B_{\beta\gamma} \frac{\partial}{\partial \beta} + \frac{1}{\beta} \frac{\partial}{\partial \gamma} \sqrt{\frac{r}{w}} \sin 3\gamma B_{\beta\beta} \frac{\partial}{\partial \gamma} \Big] \Big\}, \end{aligned} \quad (2)$$

$$\hat{T}_{\text{rot}} = \frac{1}{2} \sum_{k=1}^3 \frac{\hat{j}_k^2}{\mathcal{I}_k}. \quad (3)$$

\hat{j}_k denotes the components of the angular momentum in the body-fixed frame of a nucleus, and both the mass parameters $B_{\beta\beta}$, $B_{\beta\gamma}$, $B_{\gamma\gamma}$ and the moments of inertia \mathcal{I}_k depend on the quadrupole deformation variables β and γ . Two additional quantities that appear in \hat{T}_{vib} , namely, $r = B_1 B_2 B_3$ (see Ref. [68] for the definition of B_k), and $w = B_{\beta\beta} B_{\gamma\gamma} - B_{\beta\gamma}^2$, determine the volume element in the collective space.

The 5DCH describes quadrupole vibrations, rotations, and the coupling of these collective modes. The corresponding eigenvalue equation is solved by expanding the eigenfunctions on a complete set of basis functions that depend on the deformation variables β and γ , and the Euler angles [85]. And thus we obtain the energy spectrum E_α^I and collective wave functions

$$\Psi_\alpha^{IM}(\beta, \gamma, \Omega) = \sum_{K \in \Delta I} \psi_{\alpha K}^I(\beta, \gamma) \Phi_{MK}^I(\Omega), \quad (4)$$

where M and K are the projections of angular momentum I on the third axis in the laboratory and intrinsic frames, respectively, and α denotes the other quantum number. Using the collective wave functions, various observables such as the $E2$ transition probabilities can be calculated,

$$B(E2; \alpha' I \rightarrow \alpha' I') = \frac{1}{2I+1} |\langle \alpha' I' | \hat{M}(E2) | \alpha I \rangle|^2, \quad (5)$$

where $\hat{M}(E2)$ is the electric-quadrupole operator.

In the framework of 5DCH-CDFT, the collective parameters of 5DCH, including the mass parameters $B_{\beta\beta}$, $B_{\beta\gamma}$, and $B_{\gamma\gamma}$, the moments of inertia \mathcal{I}_k , and the collective potential V_{coll} , are all determined microscopically from the constrained triaxial CDFT calculations. The entire map of the energy surface as a function of the quadrupole deformations is obtained by imposing constraints on the axial and triaxial mass quadrupole moments:

$$E_{\text{tot}} + \sum_{\mu=0,2} C_{2\mu} (\langle \hat{Q}_{2\mu} \rangle - q_{2\mu})^2. \quad (6)$$

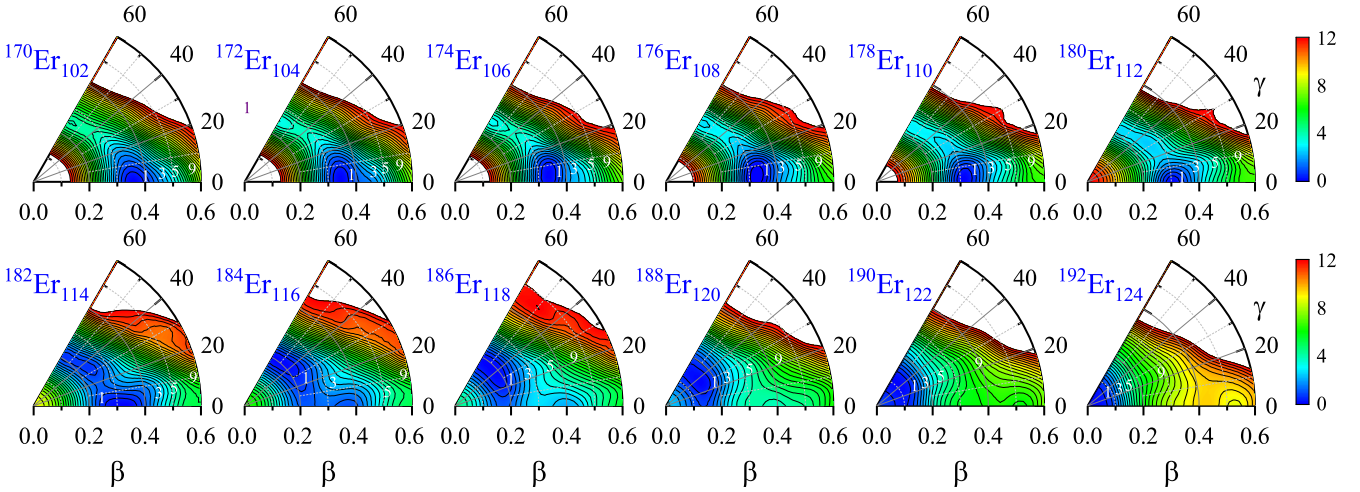


FIG. 1. Potential-energy surfaces of the even-even $^{170-192}\text{Er}$ isotopes in the (β, γ) plane, calculated by constrained triaxial RMF + BCS with the PC-PK1 functional [cf. Eq. (6)]. All energies are normalized with respect to the binding energy of the absolute minimum. The energy difference between neighboring contours is 0.5 MeV. (The radial, γ axes are given in units of degrees.)

The total energy reads

$$E_{\text{tot}} = \int [\varepsilon_{\text{RMF}}(\mathbf{r}) + \varepsilon_{\text{pair}}^p(\mathbf{r}) + \varepsilon_{\text{pair}}^n(\mathbf{r})] d\mathbf{r} + E_{\text{c.m.}}, \quad (7)$$

where $\varepsilon_{\text{RMF}}(\mathbf{r})$ and $\varepsilon_{\text{pair}}^{p(n)}(\mathbf{r})$ denote the self-consistent relativistic mean-field (RMF) energy and the pairing energies, respectively. $E_{\text{c.m.}}$ is the center-of-mass correction to the total energy. The detailed formalism can be found in Ref. [68].

$\langle \hat{Q}_{2\mu} \rangle$ in Eq. (6) denotes the expectation value of the mass quadrupole operator:

$$\langle \hat{Q}_{20} \rangle = 2z^2 - x^2 - y^2 \quad \text{and} \quad \langle \hat{Q}_{22} \rangle = x^2 - y^2. \quad (8)$$

$q_{2\mu}$ is the constrained value of the multipole moment and $C_{2\mu}$ is the corresponding stiffness constant [86].

The constrained CDFT solutions for the single-quasiparticle energies and wave functions for the entire energy surface provide the microscopic input for calculation of the collective parameters. The moments of inertia are calculated with Inglis-Belyaev formula [87,88] and the mass parameters with the cranking approximation [89]. The collective potential V_{coll} is obtained by subtracting the zero-point energy corrections [89] from the total energy that corresponds to the solution of constrained triaxial CDFT.

III. RESULTS AND DISCUSSION

In the calculations of CDFT, the relativistic point-coupling energy functional PC-PK1 [54] and a separable pairing force [90] are adopted in the particle-hole and particle-particle channels, respectively. The Dirac equation is solved by expanding the Dirac spinor in terms of the three-dimensional (3D) harmonic-oscillator basis with 16 major shells. Parity, D2 symmetry, and time-reversal invariance are imposed in the quadrupole deformation constrained relativistic mean-field plus BCS (RMF + BCS) calculation, from which the triaxial mean-field states with deformation parameters $\beta \in [0.0, 0.8]$ and $\gamma \in [0^\circ, 60^\circ]$ and the step sizes $\beta = 0.05$, $\gamma = 6^\circ$ are generated. More details about the mean-field calculations can

be found in Refs. [68,91]. In the collective Hamiltonian (1), the mass parameters and moments of inertia are determined using the cranking-approximated formalism based on the axial and triaxial mean-field states [68]. The diagonalization of the 5DCH yields the spectroscopic properties of low-lying states, including energies and electric multipole transition strengths calculated with the collective wave functions [68]. Here we note that we do not introduce a scaling factor (adjusted to the excitation energy of the 2_1^+ state) for the moments of inertia in the calculations.

In the following, the theoretical calculations for six even-even Er, Yb, Hf, W, Os, Pt isotopes with $102 \leq N \leq 124$ are presented, including potential-energy surfaces (PESs), characteristic collective observables deduced from low-lying spectra, odd-even energy staggering in the γ bands, and spectra for possible triaxial deformed and shape coexisting nuclei.

A. Potential-energy surfaces

Figures 1–6 display the PESs of the even-even Er, Yb, Hf, W, Os, and Pt isotopes with neutron number $102 \leq N \leq 124$ in the (β, γ) plane, respectively. They are obtained by the constrained triaxial CDFT calculations (6) using the relativistic PC-PK1 functional. For each nucleus, all energies are normalized with respect to the binding energy of the corresponding absolute minimum. For Er and Yb isotopic chains, Figs. 1 and 2 illustrate a shape evolution from well-deformed prolate shape near neutron number $N = 102$, to prolate-oblate shape coexistence at $N = 114, 116$, then to oblate shape at $N = 118, 120$, and finally to near spherical shape at $N = 122, 124$. Starting from $N = 114$ isotones, ^{182}Er and ^{184}Yb , a certain degree of triaxiality develops. For Hf, W, and Os isotopic chains, the PESs illustrate a shape evolution from well-deformed prolate shape, to γ -soft, then to triaxial deformed with shallow triaxial minimum, and finally to near spherical shape. Specifically, the nuclei with triaxial minima are ^{192}Hf , ^{194}W , and $^{190-196}\text{Os}$. In Fig. 6, a prolate-oblate-spherical shape transition is predicted in Pt isotopes. It is

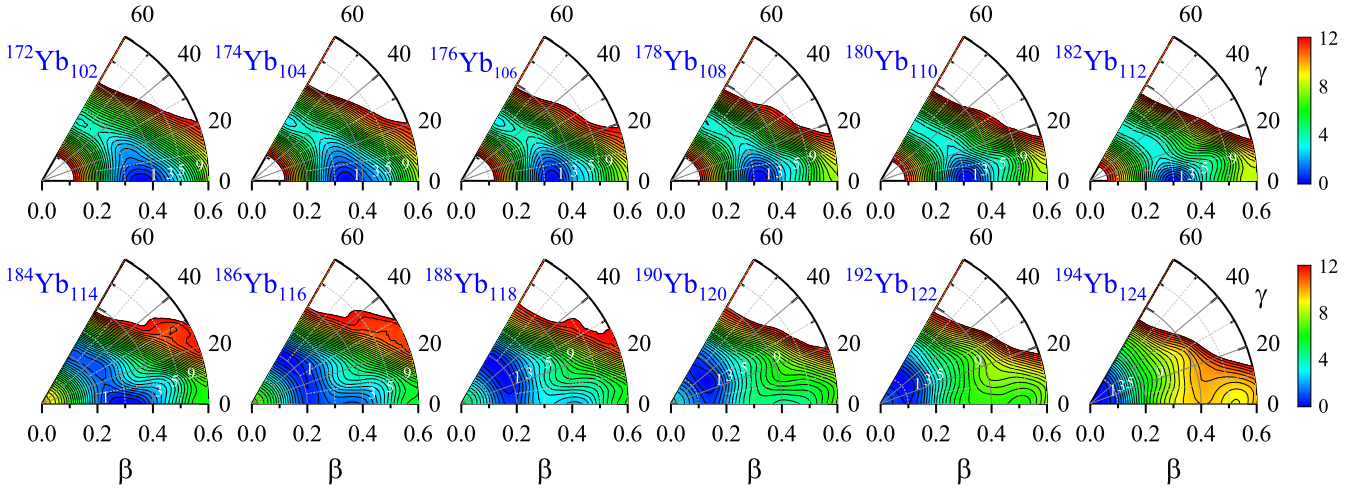


FIG. 2. Same as Fig. 1, but for Yb isotopes.

notable that, for $^{188-196}\text{Pt}$, the prolate or oblate minima are rather extended in the γ direction. For the heavier isotopes of the six isotopic chains, one notes that a large deformed prolate minimum with $\beta \gtrsim 0.4$ is predicted by the RMF + BCS calculation.

Similar topographies of the PESs and shape evolution in this region have also been obtained in studies based on the Hartree-Fock-Bogoliubov (HFB) with the Gogny D1S [22,23,38] and D1M [32] interactions, and Hartree-Fock plus BCS (HF + BCS) with the Skyrme SLy4 interaction [38]. In particular, the prolate-oblate shape coexistence in Er and Yb isotopes with neutron number $N \approx 116$ predicted here are confirmed by HFB (HF + BCS) calculations with both Gogny and Skyrme interactions. For the higher-Z isotopes, some differences can be found in the exact locations of the equilibrium triaxial minima and the corresponding triaxial deformation energies.

B. Characteristic collective observables

Starting from constrained self-consistent solutions, the collective parameters that determine 5DCH are calculated as

functions of the deformation parameters β and γ , the diagonalization of the resulting Hamiltonian yields the excitation energies and collective wave functions. In Fig. 7, we analyze the evolution of several quantities deduced from low-lying spectra to characterize transitions between different shapes as functions of the neutron number: the energy ratios $R_{42} = E(4_1^+)/E(2_1^+)$, $R_{4\gamma} = E(2_\gamma^+)/E(4_1^+)$, the excitation energies $E(0_2^+)$ of the 0_2^+ states, the $B(E2; 2_1^+ \rightarrow 0_1^+)$ values, the spectroscopic quadrupole moments $Q_s(2_1^+)$, and the $B(E2)$ ratios $R_B = B(E2; 2_\gamma^+ \rightarrow 2_1^+)/B(E2; 2_1^+ \rightarrow 0_1^+)$. Where available, the results are shown in comparison with available data [92,93]. The ratio R_{42} is probably the simplest and best-studied measure for the evolution of collectivity to distinguish between an axially symmetric deformed rotor ($R_{42} = 3.33$), a spherical vibrational nucleus ($R_{42} = 2.0$), and a triaxial rotor ($R_{42} = 2.5$). The ratio $R_{4\gamma}$ presents the location of the bandhead of the quasi- γ band 2_γ^+ relative to the 4_1^+ excitation energy. Since in many γ -soft nuclei the 2_γ^+ level lies quite close to the 4_1^+ level, the overall trend of the ratio $R_{4\gamma}$ can help to measure the γ softness. The sign of the spectroscopic quadrupole moment $Q_s(2_1^+)$ is related to the

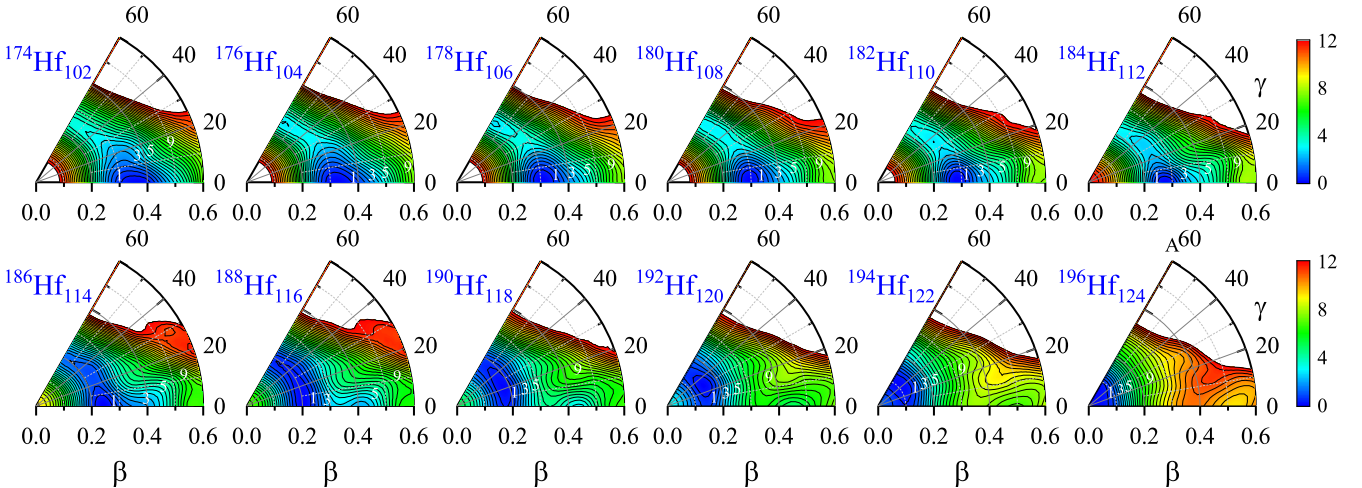


FIG. 3. Same as Fig. 1, but for Hf isotopes.

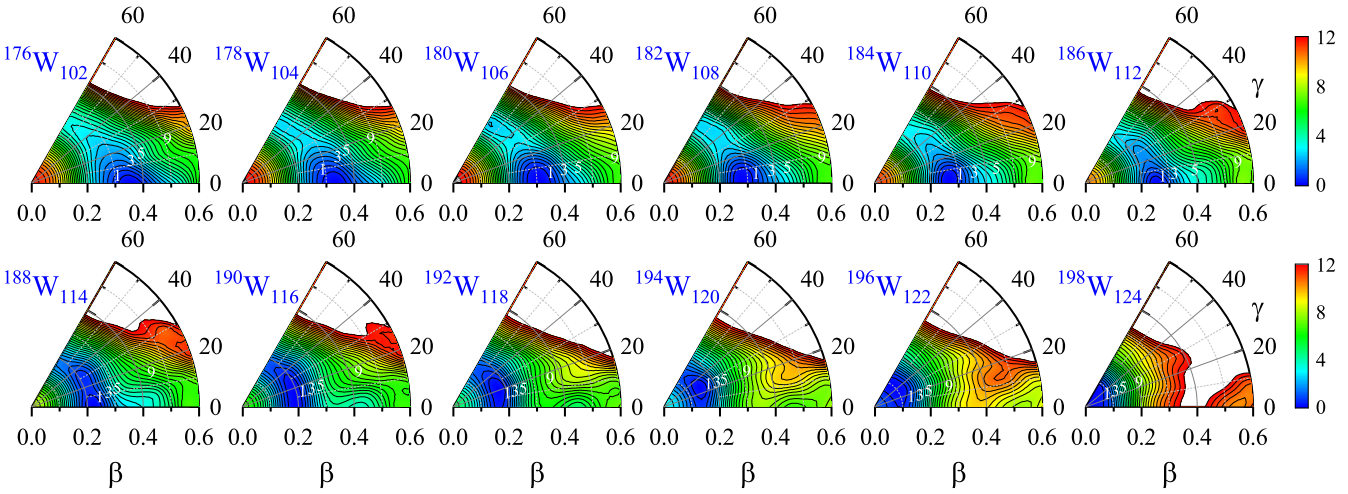


FIG. 4. Same as Fig. 1, but for W isotopes.

type of quadrupole deformation. For axially deformed case, a negative value corresponds to a prolate and a positive value to an oblate deformation in the intrinsic frame of the nucleus. The ratio $R_B = B(E2; 2^+_2 \rightarrow 2^+_1)/B(E2; 2^+_1 \rightarrow 0^+_1)$ also shows a certain sensitivity to the evolution of shapes, e.g., $R_B = 0$ for an axially symmetric deformed rotor, $R_B = 10/7$ for a γ -soft rotor, and $R_B = 2$ for a spherical shape.

For Er and Yb isotopic chains, lacking of experimental data, the calculated R_{42} in Fig. 7(a) starts from ≈ 3.3 characterized for an axially deformed rotor, drops rapidly to ≈ 2.6 at $N \approx 114$, and decreases gradually to ≈ 2.0 at $N = 124$ characterized for a spherical shape as the neutron number increases. The $R_{4\gamma}$ in Fig. 7(b) jumps dramatically from $\gtrsim 3.0$ to $\lesssim 1.0$ at $N = 114$, which demonstrates that the shapes of the heavier isotopes with $N \geq 114$ are γ -soft around the ground state. Rapid evolution is also found in the $B(E2; 2^+_2 \rightarrow 0^+_1)$ values, the spectroscopic quadrupole moments $Q_s(2^+_1)$, and the $B(E2)$ ratio $B(E2; 2^+_2 \rightarrow 2^+_1)/B(E2; 2^+_1 \rightarrow 0^+_1)$ at $N \approx 114$. Furthermore, the positive $Q_s(2^+_1)$ at $N \approx 118$ in Fig. 7(e) indi-

cate that these isotopes could be oblate deformed. Meanwhile, very low-lying 0^+_2 states in Fig. 7(c) are predicted at $N \approx 114$, supporting the shape coexistence phenomena shown in the PESs in Figs. 1 and 2. The evolution of all the collective observables characterizes a shape transition from an axially deformed rotor to prolate-oblate shape coexistence, then to oblate shape, and finally to a near spherical shape along the Er and Yb isotopic chains, which is consistent with the evolution of the potential-energy surfaces in Figs. 1 and 2.

For Hf, W, and Os isotopic chains, the calculated collective observables are in reasonable agreement with the available data except $E(0^+_2)$ and $B(E2; 2^+_1 \rightarrow 0^+_1)$ of the lighter isotopes where the theoretical results overestimate the data. The collective observables in these three isotopic chains present a similar shape evolution as that in Er and Yb isotopes, but the rapid shape transition around $N = 114$ in the latter becomes rather moderate. Moreover, the oblate shapes predicted in Er and Yb nuclei with $N \approx 118$ are not suggested in the heavier isotones since their spectroscopic quadrupole moments of 2^+_1 states are negative. Moving to Pt isotopes, the

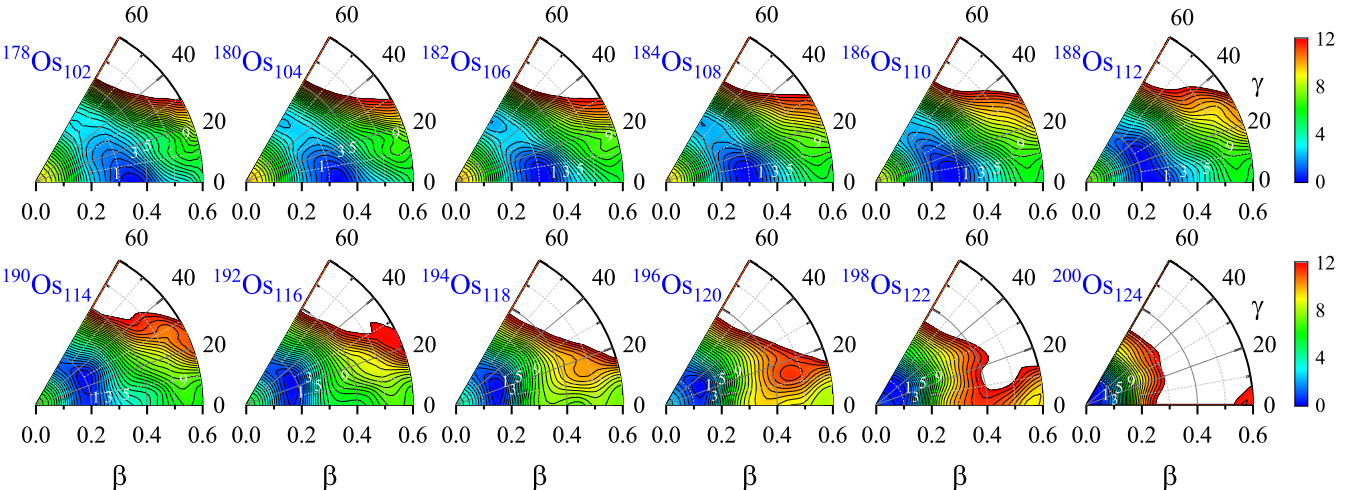


FIG. 5. Same as Fig. 1, but for Os isotopes.

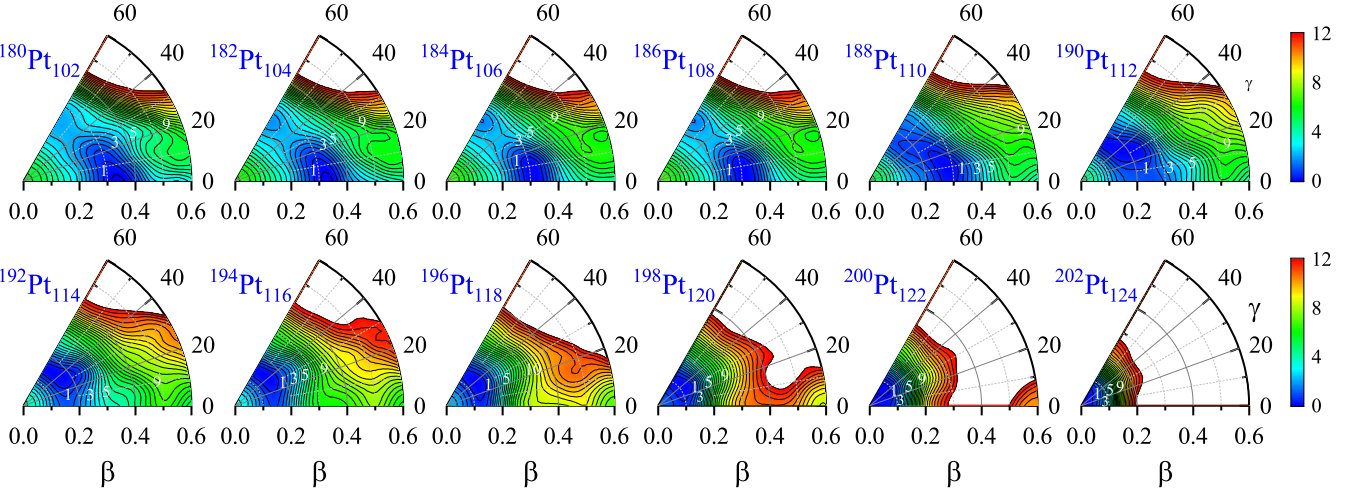


FIG. 6. Same as Fig. 1, but for Pt isotopes.

theoretical results reproduce the data for heavier nuclei but overestimate those of lighter nuclei. This could be because the axial deformation β for lighter Pt isotopes predicted by PC-PK1 functional is too large (cf. Fig. 6). It is notable that the prolate-oblate shape phase transition with the critical point at $N \approx 110$ is strongly supported by the evolution of $E(0_2^+)$, the spectroscopic quadrupole moments $Q_s(2_1^+)$, and the $B(E2)$ ratios $B(E2; 2_2^+ \rightarrow 2_1^+)/B(E2; 2_1^+ \rightarrow 0_1^+)$.

The systematics of similar characteristic collective observables, e.g., R_{42} , $R_{4\gamma}$, and the $B(E2)$ ratio $B(E2; 2_2^+ \rightarrow 2_1^+)/B(E2; 2_1^+ \rightarrow 0_1^+)$, in Yb, Hf, W, Os, and Pt isotopes with $110 \leq N \leq 122$ have been studied by an interacting-boson-model (IBM) Hamiltonian determined from Hartree-Fock-Bogoliubov calculations with the Gogny energy density functional D1M [32] and D1S [31,35]. Moreover, the generator coordinate method (GCM) based on the Gogny D1S has also been applied to study the yrast band excitation energies, normalized to the corresponding 2_1^+ energies, for the stable and neutron-rich Os and Pt isotopes [22,23]. For the energy ratios, our theoretical results are consistent with the IBM and GCM predictions, and all the models can reproduce the rapid shape transition in Yb-Os isotopes with $110 \leq N \leq 116$. However, the R_{42} values calculated by the IBM present an increase for the heavier Yb-Os isotopes with $N \geq 118$, contrary to the experimental tendency of Os isotopes. For the $B(E2)$ ratios, the theoretical results obtained by both IBM and our model are in reasonable agreement with the available data in W and Os isotopes, while in Pt isotopes, discrepancy is found especially in the IBM calculations since the triaxial dynamics is not correctly incorporated in the model [32].

C. Energy staggering in the γ band

It is interesting to further investigate the odd-even energy staggering in the γ bands, to probe the γ deformation. Within the γ band, γ -band staggering

$$S(J) = \frac{[E(J) - E(J-1)] - [E(J-1) - E(J-2)]}{E(2_1^+)} \quad (9)$$

has been suggested as an important measure to distinguish soft or rigid triaxiality [94,95]. For a γ -rigid rotor, the γ

band should exhibit pairs of levels close in energy, $(2^+, 3^+)$, $(4^+, 5^+)$, $(6^+, 7^+)$, ... (odd spins lower in energy), while for a γ -soft collective structure a grouping of levels 2^+ , $(3^+, 4^+)$, $(5^+, 6^+)$, ... (even spins lower) should be observed. Thus, in both cases $S(J)$ shows an odd-even staggering with the increase of spin, and $S(4) > 0$ in the former case while $S(4) < 0$ in the latter case. In addition, for an ideal axially symmetric rotor, this staggering parameter is a constant $S(J) = 0.33$, while for a harmonic vibrator, it exhibits a staggering behavior with an absolute value equal to 1 and $S(4) = -1$.

Figure 8 displays the experimental and theoretical energy staggering parameter $S(J)$ as a function of spin for the γ bands in the transitional Hf, W, Os, and Pt isotopes with $108 \leq N \leq 122$ to study the triaxial shape transition and possible rigid triaxial deformation. The calculations can reproduce the experimental data for both the phases and amplitudes of the staggering behavior for most of the nuclei where the data are available. For Hf and W isotopes, the staggering parameters $S(J)$ of $^{180,182}\text{Hf}$ and $^{182,184}\text{W}$ with $N = 108, 110$ characterize for an axially symmetric rotor. While moving to $N = 112, 114$, the large amplitude of $S(J)$ and also increasing with spin indicate the rapid onset of the triaxial-soft deformation in these isotopes. As the neutron number increases further, the oscillation of $S(J)$ becomes moderate gradually and the corresponding deformation becomes weak until near spherical shape. A particular interesting nucleus is ^{194}W , where the phase of $S(J)$ at $J \geq 6\hbar$ is same as the one of a γ -rigid rotor. This is also consistent with the fact that a global triaxial minimum ($\beta, \gamma \approx (0.15, 30^\circ)$) is observed in the corresponding PESs (cf. Fig. 4).

Similar to the lighter Hf and W isotopes, the experimental staggering parameters $S(J)$ of $^{184,186}\text{Os}$ characterize an axially symmetric rotor. Weak oscillated $S(J)$ is also observed in $^{188,190}\text{Os}$ but the phase at high spins tends to the one of a γ -rigid rotor, namely, negative for odd spins and positive for even spins. Furthermore, the oscillation at high spins is enhanced rapidly for the heavier Os isotopes $^{192-198}\text{Os}$, which implies to the onset of a triaxial minimum in these nuclei (cf. Fig. 5).

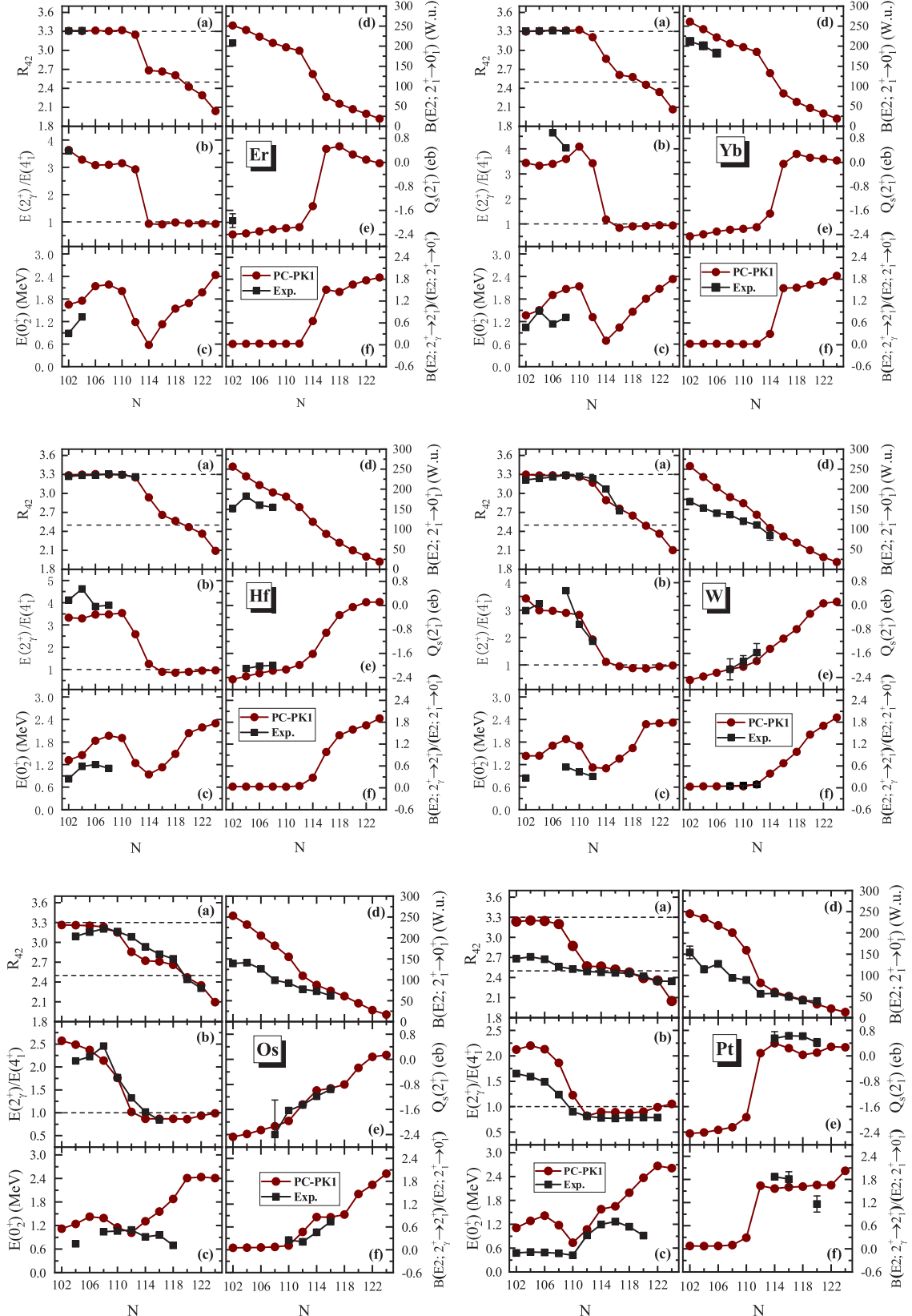


FIG. 7. Spectroscopic properties of the six even-even Er, Yb, Hf, W, Os, and Pt isotopes with $102 \leq N \leq 124$ plotted as functions of neutron number: (a) evolution of $R_{42} = E(4_1^+)/E(2_1^+)$, (b) $E(2_1^+)/E(4_1^+)$, (c) the excitation energies of the 0_2^+ states $E(0_2^+)$ (in MeV), (d) the $B(E2; 2_1^+ \rightarrow 0_1^+)$ values (in Weisskopf units), (e) spectroscopic quadrupole moments $Q_s(2_1^+)$ (in eb), and (f) the $B(E2)$ ratios $R_B = B(E2; 2_1^+ \rightarrow 2_1^+)/B(E2; 2_1^+ \rightarrow 0_1^+)$ calculated by 5DCH-CDFT with the PC-PK1 functional, in comparison with available data [92,93].

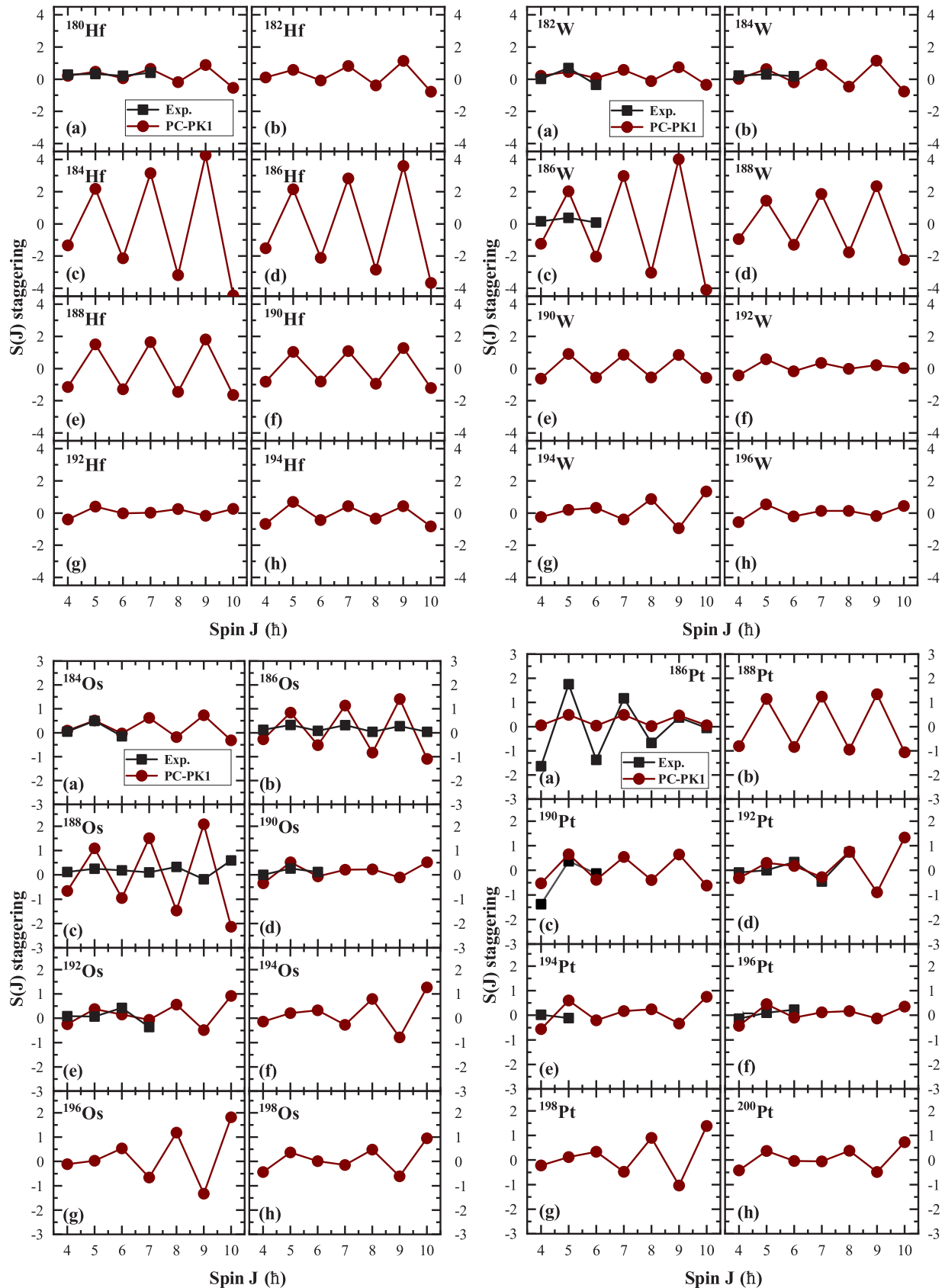


FIG. 8. Staggering parameters $S(J)$ of even-even Hf, W, Os, and Pt isotopic chains calculated by 5DCH-CDFT with PC-PK1 functional in comparison with the available data [92].

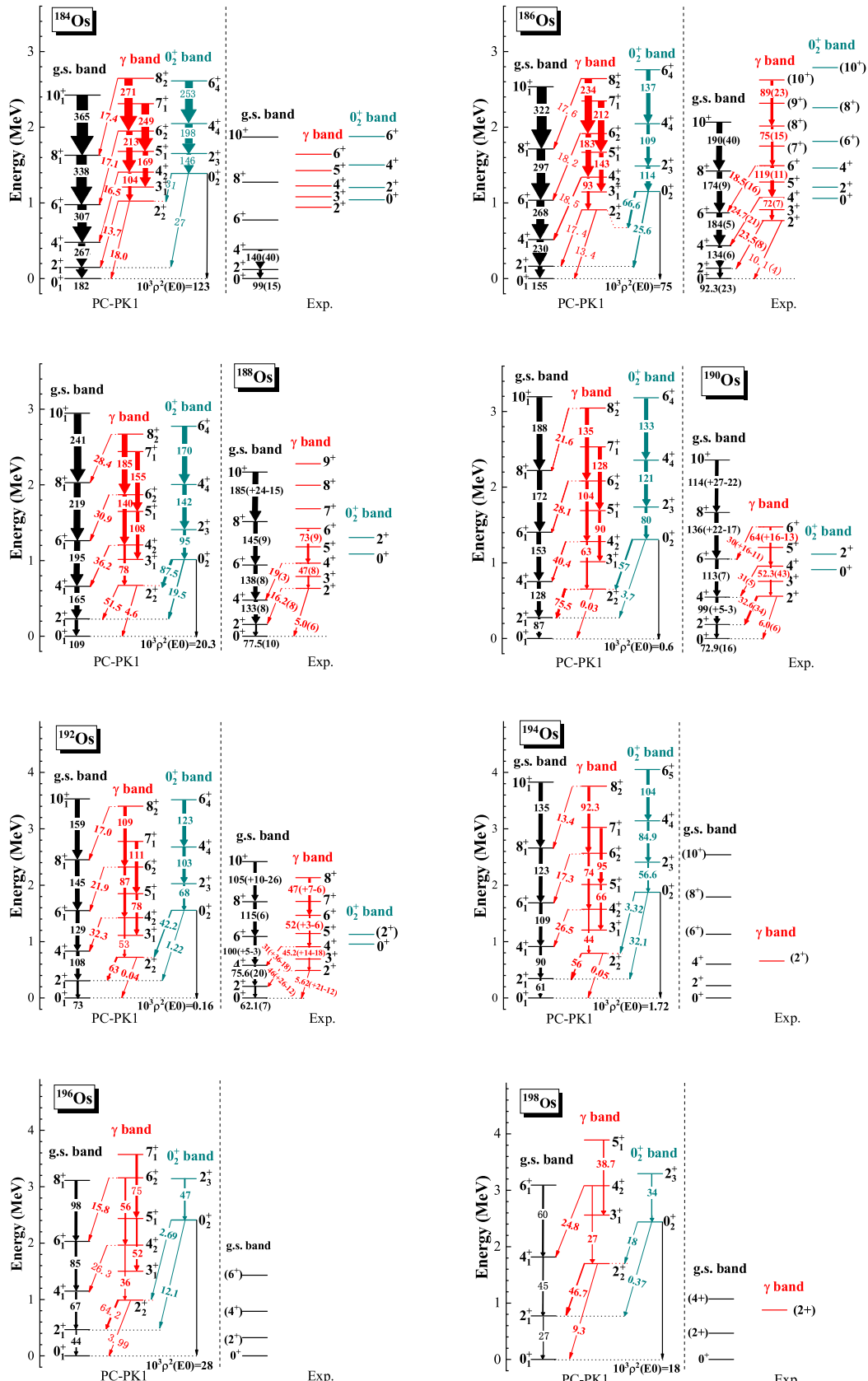


FIG. 9. Calculated excitation energies (in MeV), $\rho^2(E0; 0_2^+ \rightarrow 0_1^+)$, intraband and interband $B(E2)$ values (in Weisskopf units) for ground-state bands, γ bands, and 0_2^+ bands in the even-even $^{184-198}\text{Os}$ isotopes by 5DCH-CDFT (PC-PK1), in comparison with the experimental data [92].

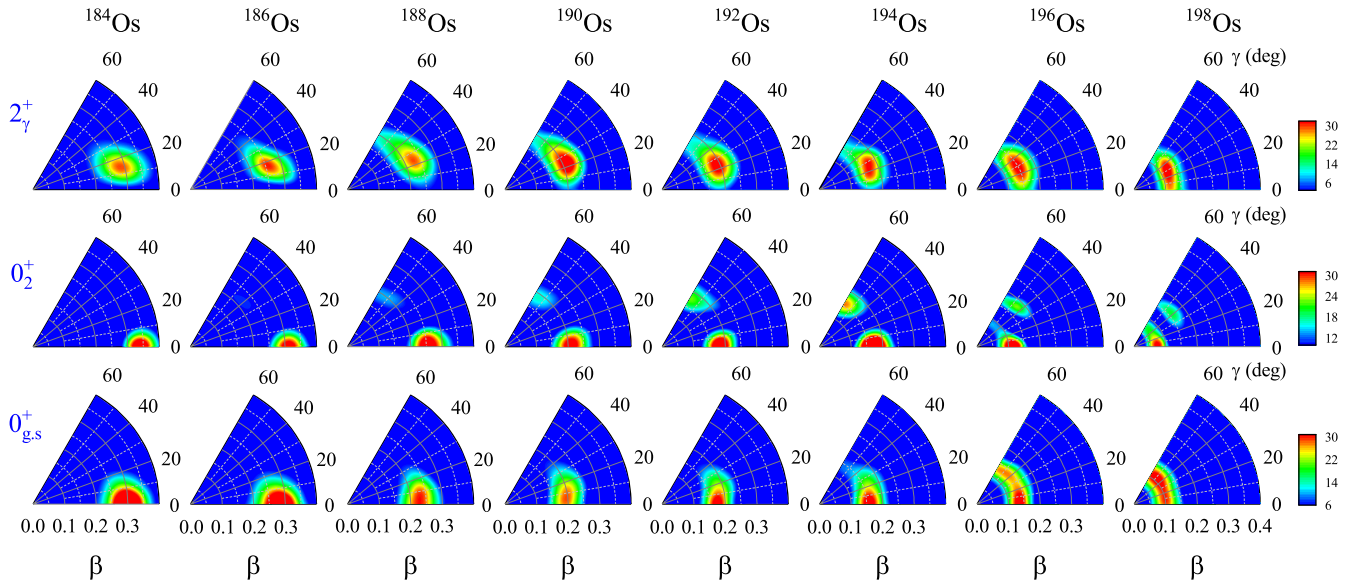


FIG. 10. Probability density distributions $\rho_{I\alpha}(\beta, \gamma)$ in the (β, γ) plane for the $0_{g.s.}^+$, 0_2^+ , and 2_γ^+ collective states in the even-even $^{184-198}\text{Os}$ isotopes. (The radial, γ axes are given in units of degrees.)

The experimental staggering parameters $S(J)$ of ^{186}Pt demonstrate the γ -soft feature for low-spin states and approaching to prolate for high-spin states (experimental data are close to theoretical results for high spins). By adding two or four neutrons, $^{188,190}\text{Pt}$ are dominated by the γ -soft shape. The evolution of $S(J)$ for heavier Pt isotopes becomes quite complicated. By combining the PESs in Fig. 6 and collective observables, especially $R_{4\gamma}$ and $Q_s(2_1^+)$ in Fig. 7, one can conclude that the heavier Pt isotopes $^{192-200}\text{Pt}$ have (weak) oblate shape but extended to triaxial deformation.

D. Low-lying spectra and probability density distributions for Os isotopes

Since the transitional Os isotopes have plenty of experimental data for low-lying spectra, here in Fig. 9 we compare our theoretical results of $^{184-198}\text{Os}$ with the available data in detail. The levels are grouped into ground-state (g.s.) bands, γ bands, and 0_2^+ bands according to the predominant K components and dominant decay patterns. The $\rho^2(E0; 0_0^+ \rightarrow 0_1^+)$, intraband and interband $B(E2)$ values are also shown in the figure. In general, the 5DCH calculations can reproduce the collective structure, although the theoretical spectra are stretched. This is because the adiabatic approximation is adopted in the present 5DCH-CDFT framework, namely, the collective parameters, especially the moments of inertia, do not depend on the angular momentum. To solve this problem, one could construct 5DCH based on the cranking CDFT framework [96], and such an extension of the model is in progress. For the electric-quadrupole transitions, the theoretical results are generally larger than the data, especially for the lighter Os isotopes. This is probably due to the overestimation of the quadrupole deformation in the calculations (cf. Fig. 5). Note that, starting from ^{190}Os , the signatures of the triaxiality including the low-lying γ bandhead, the enhanced interband

transitions $B(E2; 2_\gamma^+ \rightarrow 2_1^+)$, and the γ band staggers (cf. Fig. 8) are all reproduced quite well. This may imply that the predicted level structure and electric transitions for the neutron-rich $^{194-198}\text{Os}$ isotopes are somehow reliable.

The probability density distribution of the collective state, which takes the following form:

$$\rho_{I\alpha}(\beta, \gamma) = \sum_{K \in \Delta I} |\psi_{\alpha K}^I(\beta, \gamma)|^2 \beta^3, \quad (10)$$

with the normalization

$$\int_0^\infty \beta d\beta \int_0^{2\pi} \rho_{I\alpha}(\beta, \gamma) |\sin(3\gamma)| d\gamma = 1, \quad (11)$$

could give a further insight into the shape evolution with spin and isospin [81,97]. Here the density distributions for the $0_{g.s.}^+$, 0_2^+ , and 2_γ^+ states in $^{184-198}\text{Os}$ are depicted in Fig. 10. For the ground states $0_{g.s.}^+$, the peaks of collective wave functions shift to the smaller β gradually and extend in the γ direction until a γ -soft rotor as the neutron number increases. 0_2^+ states possess similar dominated configurations as those of corresponding $0_{g.s.}^+$, but a mixing with an oblate configuration is observed for heavier Os isotopes. For the 2_γ^+ states, the density distributions present a clear evolution from γ vibration of an axially deformed rotor in ^{184}Os to triaxial deformed shape in $^{190-196}\text{Os}$, where the peaks are concentrated in $\gamma = 20^\circ-40^\circ$, and finally to γ -soft rotor in ^{198}Os .

E. Prolate-oblate shape coexistence in neutron-rich Er and Yb isotopes

Finally, Fig. 11 illustrates the calculated low-lying spectra for ^{184}Er and ^{186}Yb , candidates for prolate-oblate shape coexistence. In addition, we also plot the probability density distributions in the (β, γ) plane for the bandheads. It is remarkable that a multishape coexistence of medium-deformed oblate shape, medium- and large-deformed prolate shapes is

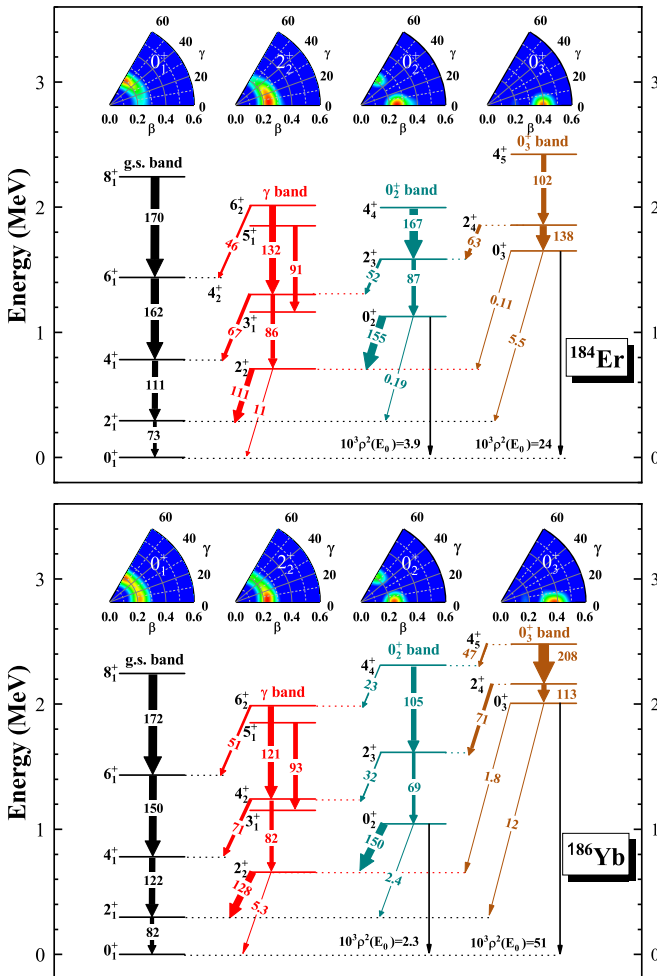


FIG. 11. The low-lying spectra of ^{184}Er (upper panel) and ^{186}Yb (lower panel) calculated with 5DCH-CDFT based on PC-PK1 functional. The probability density distributions in the (β, γ) plane for the bandheads are also shown by the contour plots. (The radial, γ axes are given in units of degrees.)

predicted in both nuclei. The ground-state (g.s.) band corresponds to an oblate but γ -soft geometric shape, which is also reflected in the low-lying γ band and strong mixing between γ band and g.s. band [large interband $B(E2)$ transitions]. In contrast, the 0_2^+ and 0_3^+ bands are predicted to be medium- and large-deformed prolate shapes with $\beta \approx 0.25$ and 0.4, respectively, and consequently the interband $B(E2)$ and $\rho(E0)$ transitions from 0_2^+ or 0_3^+ bands to the g.s. band are quite small due to the weak mixing between them.

IV. SUMMARY

We have analyzed the shape transition and possible occurrence of low-energy shape coexistence and rigid triaxial

deformation in the six even-even Er, Yb, Hf, W, Os, and Pt isotopic chains with the neutron number $102 \leq N \leq 124$. The potential-energy surfaces, low-lying spectra, and characteristic collective observables have been studied by solving a five-dimensional collective Hamiltonian with parameters determined from the relativistic energy density functional PC-PK1 and a separable finite-range pairing interaction. The potential-energy surfaces display a transition from prolate to oblate or triaxial, and then to near spherical shapes as the neutron number increases. In particular, the Er and Yb nuclei with $N = 114, 116$ exhibit coexisting low-energy axially deformed prolate and oblate minima, while triaxial minima are observed in ^{192}Hf , ^{194}W , and $^{190-196}\text{Os}$.

The SCMF deformation-constrained solutions provide a microscopic input for the parameters of the 5D collective Hamiltonian that has been used to calculate spectroscopic properties of low-energy states. The 5DCH model calculations reproduce the empirical isotopic trend of the characteristic collective observables: $E(4_1^+)/E(2_1^+)$, $E(2_\gamma^+)/E(4_1^+)$, the excitation energy of 0_2^+ state $E(0_2^+)$, $B(E2; 2_1^+ \rightarrow 0_1^+)$, the spectroscopic quadrupole moment $Q_s(2_1^+)$, the ratio $B(E2; 2_\gamma^+ \rightarrow 2_1^+)/B(E2; 2_1^+ \rightarrow 0_1^+)$, and energy staggering in the γ band. The evolution of the collective observables confirms the overall shape transition in this region. Specifically, a rapid shape transition between prolate and oblate shapes is predicted in Er and Yb isotopic chains while it becomes smooth for higher-Z isotopic chains and signature for rigid triaxial deformation is found in the transitional isotopes, e.g., ^{194}W and $^{192-196}\text{Os}$. Finally, the calculated low-lying spectra and probability density distributions for Os isotopes as well as the shape-coexisting candidates ^{184}Er and ^{186}Yb are illustrated. The triaxial deformation in $^{192-196}\text{Os}$ is further confirmed by analyzing the probability density distributions of γ bandhead. Moreover, a remarkable multishape coexistence of medium-deformed oblate shape, medium- and large-deformed prolate shapes is predicted in ^{184}Er and ^{186}Yb .

ACKNOWLEDGMENTS

This work has been supported in part by the NSFC under Grants No. 11875225, No. 11765015, No. 11790325, No. 12005109, No. 12005082, and No. 11905175, the Fok Ying-Tong Education Foundation, Joint Fund Project of Education Department in Guizhou Province (No. Qian Jiao He KY Zi[2018]433), the science and technology program foundation of Guizhou province (Qian KeHe Platform Talents[2019]QNSYXM-03), Jiangxi Provincial Natural Science Foundation 20202BAB211008, Jiangxi Normal University (JXNU) Initial Research Foundation Grant to Doctor (12019504), and the Young Talents Program under JXNU (12019870).

[1] K. Heyde and J. L. Wood, *Rev. Mod. Phys.* **83**, 1467 (2011).

[2] K. Wrzosek-Lipska and L. P. Gaffney, *J. Phys. G* **43**, 024012 (2016).

- [3] F. Iachello, *Phys. Rev. Lett.* **87**, 052502 (2001).
- [4] F. Iachello, *Phys. Rev. Lett.* **85**, 3580 (2000).
- [5] J. Jolie, R. F. Casten, P. von Brentano, and V. Werner, *Phys. Rev. Lett.* **87**, 162501 (2001).
- [6] R. F. Casten, *Nat. Phys.* **2**, 811 (2006).
- [7] P. Cejnar and J. Jolie, *Prog. Part. Nucl. Phys.* **62**, 210 (2009).
- [8] P. Cejnar, J. Jolie, and R. F. Casten, *Rev. Mod. Phys.* **82**, 2155 (2010).
- [9] C. B. Li, X. G. Wu, X. F. Li, C. Y. He, Y. Zheng, G. S. Li, S. H. Yao, S. P. Hu, H. W. Li, J. L. Wang, J. J. Liu, C. Xu, J. J. Sun, and W. W. Qu, *Phys. Rev. C* **86**, 057303 (2012).
- [10] M. Rudigier, K. Nomura, M. Dannhoff, R.-B. Gerst, J. Jolie, N. Saed-Samii, S. Stegemann, J.-M. Régis, L. M. Robledo, R. Rodríguez-Guzmán, A. Blazhev, C. Fransen, N. Warr, and K. O. Zell, *Phys. Rev. C* **91**, 044301 (2015).
- [11] C. Wheldon, J. Garcés Narro, C. J. Pearson, P. H. Regan, Z. Podolyák, D. D. Warner, P. Fallon, A. O. Macchiavelli, and M. Cromaz, *Phys. Rev. C* **63**, 011304(R) (2000).
- [12] N. Alkhomashi, P. H. Regan, Zs. Podolyák, S. Pietri, A. B. Garnsworthy, S. J. Steer, J. Benlliure, E. Casarejos, R. F. Casten, J. Gerl, H. J. Wollersheim, J. Grebosz, G. Farrelly, M. Gorska, I. Kojouharov, H. Schaffner, A. Algora, G. Benzoni, A. Blazhev, P. Boutachkov *et al.*, *Phys. Rev. C* **80**, 064308 (2009).
- [13] Zs. Podolyák, P. H. Regan, M. Pfützner, J. Gerl, M. Hellström, M. Caamaño, P. Mayet, Ch. Schlegel, A. Aprahamian, J. Benlliure, A. M. Bruce, P. A. Butler, D. Cortina Gil, D. M. Cullen, J. Döring, T. Enqvist, F. Rejmund, C. Fox, J. Garcés Narro, H. Geissel *et al.*, *Phys. Lett. B* **491**, 225 (2000).
- [14] P. Bond, R. Casten, D. Warner, and D. Horn, *Phys. Lett. B* **130**, 167 (1983).
- [15] Zs. Podolyák, S. J. Steer, S. Pietri, F. R. Xu, H. L. Liu, P. H. Regan, D. Rudolph, A. B. Garnsworthy, R. Hoischen, M. Gorska, J. Gerl, H. J. Wollersheim, T. Kurtukian-Nieto, G. Benzoni, T. Shizuma, F. Becker, P. Bednarczyk, L. Cáceres, P. Doornenbal, H. Geissel *et al.*, *Phys. Rev. C* **79**, 031305 (2009).
- [16] G. S. Li, M. L. Liu, X. H. Zhou, Y. H. Zhang, Y. X. Liu, N. T. Zhang, W. Hua, Y. Zheng, Y. D. Fang, S. Guo, J. G. Wang, Y. H. Qiang, B. Ding, L. Ma, M. Oshima, Y. Toh, M. Koizumi, A. Osa, Y. Hatsukawa, and M. Sugawara, *Phys. Rev. C* **89**, 054303 (2014).
- [17] S. G. Wahid, S. K. Tandel, P. Chowdhury, R. V. F. Janssens, M. P. Carpenter, T. L. Khoo, F. G. Kondev, T. Lauritsen, C. J. Lister, D. Seweryniak, and S. Zhu, *Phys. Rev. C* **92**, 054323 (2015).
- [18] S. K. Tandel, S. G. Wahid, P. Chowdhury, R. V. F. Janssens, M. P. Carpenter, T. L. Khoo, F. G. Kondev, T. Lauritsen, C. J. Lister, D. Seweryniak, and S. Zhu, *Phys. Lett. B* **750**, 225 (2015).
- [19] S. J. Steer, Z. Podolyák, S. Pietri, M. Gorska, H. Grawe, K. H. Maier, P. H. Regan, D. Rudolph, A. B. Garnsworthy, R. Hoischen, J. Gerl, H. J. Wollersheim, F. Becker, P. Bednarczyk, L. Cáceres, P. Doornenbal, H. Geissel, J. Grebosz, A. Kelic, I. Kojouharov *et al.*, *Phys. Rev. C* **84**, 044313 (2011).
- [20] A. I. Morales, J. Benlliure, M. Gorska, H. Grawe, S. Verma, P. H. Regan, Z. Podolyák, S. Pietri, R. Kumar, E. Casarejos, A. Algora, N. Alkhomashi, H. Alvarez-Pol, G. Benzoni, A. Blazhev, P. Boutachkov, A. M. Bruce, L. S. Cáceres, I. J. Cullen, A. M. Denis Bacelar, P. Doornenbal *et al.*, *Phys. Rev. C* **88**, 014319 (2013).
- [21] P. J. R. Mason, Z. Podolyák, N. Mărginean, P. H. Regan, P. D. Stevenson, V. Werner, T. Alexander, A. Algora, T. Alharbi, M. Bowry, R. Britton, A. M. Bruce, D. Bucurescu, M. Bunce, G. Căta-Danil, I. Căta-Danil, N. Cooper, D. Deleanu, D. Delion, D. Filipescu *et al.*, *Phys. Rev. C* **88**, 044301 (2013).
- [22] P. R. John, V. Modamio, J. J. Valiente-Dobón, D. Mengoni, S. Lunardi, T. R. Rodríguez, D. Bazzacco, A. Gadea, C. Wheldon, T. Alexander, G. de Angelis, N. Ashwood, M. Barr, G. Benzoni, B. Birkenbach, P. G. Bizzeti, A. M. Bizzeti-Sona, S. Bottoni, M. Bowry, A. Bracco *et al.*, *Phys. Rev. C* **90**, 021301 (2014).
- [23] P. R. John, J. J. Valiente-Dobón, D. Mengoni, V. Modamio, S. Lunardi, D. Bazzacco, A. Gadea, C. Wheldon, T. R. Rodríguez, T. Alexander, G. de Angelis, N. Ashwood, M. Barr, G. Benzoni, B. Birkenbach, P. G. Bizzeti, A. M. Bizzeti-Sona, A. M. Bizzeti-Sona, M. Bowry, A. Bracco *et al.*, *Phys. Rev. C* **95**, 064321 (2017).
- [24] N. Al-Dahan, P. H. Regan, Zs. Podolyák, P. M. Walker, N. Alkhomashi, G. D. Dracoulis, G. Farrelly, J. Benlliure, S. B. Pietri, R. F. Casten, P. D. Stevenson, W. Gelletly, S. J. Steer, A. B. Garnsworthy, E. Casarejos, J. Gerl, H. J. Wollersheim, J. Grebosz, M. Gorska, I. Kojouharov *et al.*, *Phys. Rev. C* **85**, 034301 (2012).
- [25] J. Jolie and A. Linnemann, *Phys. Rev. C* **68**, 031301(R) (2003).
- [26] P. D. Stevenson, M. P. Brine, Z. Podolyak, P. H. Regan, P. M. Walker, and J. R. Stone, *Phys. Rev. C* **72**, 047303 (2005).
- [27] P. Sarriguren, R. Rodríguez-Guzmán, and L. M. Robledo, *Phys. Rev. C* **77**, 064322 (2008).
- [28] D. Bonatsos, I. E. Assimakis, N. Minkov, A. Martinou, S. Sarantopoulou, R. B. Cakirli, R. F. Casten, and K. Blaum, *Phys. Rev. C* **95**, 064326 (2017).
- [29] A. A. Raduta and P. Buganu, *Phys. Rev. C* **88**, 064328 (2013).
- [30] A. A. Raduta and R. Budaca, *Phys. Rev. C* **84**, 044323 (2011).
- [31] K. Nomura, T. Otsuka, R. Rodríguez-Guzmán, L. M. Robledo, P. Sarriguren, P. H. Regan, P. D. Stevenson, and Z. Podolyák, *Phys. Rev. C* **83**, 054303 (2011).
- [32] K. Nomura, T. Otsuka, R. Rodríguez-Guzmán, L. M. Robledo, and P. Sarriguren, *Phys. Rev. C* **84**, 054316 (2011).
- [33] H. L. Liu, F. R. Xu, P. M. Walker, and C. A. Bertulani, *Phys. Rev. C* **83**, 067303 (2011).
- [34] J. E. García-Ramos, K. Heyde, L. M. Robledo, and R. R. Rodríguez-Guzmán, *Phys. Rev. C* **89**, 034313 (2014).
- [35] K. Nomura, T. Otsuka, R. Rodríguez-Guzmán, L. M. Robledo, and P. Sarriguren, *Phys. Rev. C* **83**, 014309 (2011).
- [36] T. Niksic, P. Ring, D. Vretenar, Y. Tian, and Z. Y. Ma, *Phys. Rev. C* **81**, 054318 (2010).
- [37] R. Rodríguez-Guzmán, P. Sarriguren, L. M. Robledo, and J. E. García-Ramos, *Phys. Rev. C* **81**, 024310 (2010).
- [38] L. M. Robledo and R. Rodríguez-Guzmán and P. Sarriguren, *J. Phys. G* **36**, 115104 (2009).
- [39] E. Clément, M. Zielińska, A. Görgen, W. Korten, S. Péru, J. Libert, H. Goutte, S. Hilaire, B. Bastin, C. Bauer, A. Blazhev, N. Bree, B. Bruyneel, P. A. Butler, J. Butterworth, P. Delahaye, A. Dijon, D. T. Doherty, A. Ekström, C. Fitzpatrick *et al.*, *Phys. Rev. Lett.* **117**, 099902 (2016).
- [40] E. Clément, M. Zielińska, A. Görgen, W. Korten, S. Péru, J. Libert, H. Goutte, S. Hilaire, B. Bastin, C. Bauer, A. Blazhev, N. Bree, B. Bruyneel, P. A. Butler, J. Butterworth, P. Delahaye, A. Dijon, D. T. Doherty, A. Ekström, C. Fitzpatrick *et al.*, *Phys. Rev. Lett.* **116**, 022701 (2016).
- [41] S. Cruz, P. C. Bender, R. Krücken, K. Wimmer, F. Ames, C. Andreoiu, R. A. E. Austin, C. S. Bancroft, R. Braid, T. Bruhn, W. N. Catford, A. Cheeseman, A. Chester, D. S. Cross, C. Aa.

- Diget, T. Drake, A. B. Garnsworthy, G. Hackman, R. Kanungo, A. Knapton *et al.*, *Phys. Lett. B* **786**, 94 (2018).
- [42] Purnima Singh, W. Korten, T. W. Hagen, A. Görzen, L. Grente, M.-D. Salsac, F. Farget, E. Clément, G. de France, T. Braueroth, B. Bruyneel, I. Celikovic, O. Delaune, A. Dewald, A. Dijon, J.-P. Delaroche, M. Girod, M. Hackstein, B. Jacquot, J. Libert, J. Litzinger *et al.*, *Phys. Rev. Lett.* **121**, 192501 (2018).
- [43] W. Witt, V. Werner, N. Pietralla, M. Albers, A. D. Ayangeakaa, B. Bucher, M. P. Carpenter, D. Cline, H. M. David, A. Hayes, C. Hoffman, R. V. F. Janssens, B. P. Kay, F. G. Kondev, W. Korten, T. Lauritsen, O. Möller, G. Rainovski, G. Savard, D. Seweryniak *et al.*, *Phys. Rev. C* **98**, 041302(R) (2018).
- [44] P. Ring, *Prog. Part. Nucl. Phys.* **37**, 193 (1996).
- [45] D. Vretenar, A. V. Afanasjev, G. A. Lalazissis, and P. Ring, *Phys. Rep.* **409**, 101 (2005).
- [46] J. Meng, H. Toki, S. G. Zhou, S. Q. Zhang, W. H. Long, and L. S. Geng, *Prog. Part. Nucl. Phys.* **57**, 470 (2006).
- [47] J. Meng, *Relativistic Density Functional for Nuclear Structure* (World Scientific, Singapore, 2016).
- [48] J. Meng, K. Sugawara-Tanabe, S. Yamaji, and A. Arima, *Phys. Rev. C* **59**, 154 (1999).
- [49] T. S. Chen, H. F. Lü, J. Meng, S. Q. Zhang, and S.-G. Zhou, *Chin. Phys. Lett.* **20**, 358 (2003).
- [50] S.-G. Zhou, J. Meng, and P. Ring, *Phys. Rev. Lett.* **91**, 262501 (2003).
- [51] H. Z. Liang, J. Meng, and S.-G. Zhou, *Phys. Rep.* **570**, 1 (2015).
- [52] W. H. Long, J. Meng, N. Van Giai, and S.-G. Zhou, *Phys. Rev. C* **69**, 034319 (2004).
- [53] W. Zhang, J. Meng, S. Q. Zhang, L. S. Geng, and H. Toki, *Nucl. Phys. A* **753**, 106 (2005).
- [54] P. W. Zhao, Z. P. Li, J. M. Yao, and J. Meng, *Phys. Rev. C* **82**, 054319 (2010).
- [55] W. Zhang, Z. P. Li, and S. Q. Zhang, *Phys. Rev. C* **88**, 054324 (2013).
- [56] J. Meng and P. Ring, *Phys. Rev. Lett.* **77**, 3963 (1996).
- [57] J. Meng and P. Ring, *Phys. Rev. Lett.* **80**, 460 (1998).
- [58] J. Meng, H. Toki, J. Y. Zeng, S. Q. Zhang, and S.-G. Zhou, *Phys. Rev. C* **65**, 041302 (2002).
- [59] J. Meng and S.-G. Zhou, *J. Phys. G* **42**, 093101 (2015).
- [60] H. Z. Liang, N. Van Giai, and J. Meng, *Phys. Rev. Lett.* **101**, 122502 (2008).
- [61] H. Z. Liang, N. V. Giai, and J. Meng, *Phys. Rev. C* **79**, 064316 (2009).
- [62] P. W. Zhao, S. Q. Zhang, J. Peng, H. Z. Liang, P. Ring, and J. Meng, *Phys. Lett. B* **699**, 181 (2011).
- [63] P. W. Zhao, J. Peng, H. Z. Liang, P. Ring, and J. Meng, *Phys. Rev. Lett.* **107**, 122501 (2011).
- [64] P. W. Zhao, J. Peng, H. Z. Liang, P. Ring, and J. Meng, *Phys. Rev. C* **85**, 054310 (2012).
- [65] P. W. Zhao, N. Itagaki, and J. Meng, *Phys. Rev. Lett.* **115**, 022501 (2015).
- [66] P. W. Zhao, S. Q. Zhang, and J. Meng, *Phys. Rev. C* **92**, 034319 (2015).
- [67] P. W. Zhao, *Phys. Lett. B* **773**, 1 (2017).
- [68] T. Nikšić, Z. P. Li, D. Vretenar, L. Próchniak, J. Meng, and P. Ring, *Phys. Rev. C* **79**, 034303 (2009).
- [69] Z. P. Li, T. Nikšić, D. Vretenar, J. Meng, G. A. Lalazissis, and P. Ring, *Phys. Rev. C* **79**, 054301 (2009).
- [70] T. Nikšić, D. Vretenar, and P. Ring, *Prog. Part. Nucl. Phys.* **66**, 519 (2011).
- [71] Z. P. Li, T. Nikšić, D. Vretenar, and J. Meng, *Phys. Rev. C* **80**, 061301(R) (2009).
- [72] Z. P. Li, T. Nikšić, D. Vretenar, P. Ring, and J. Meng, *Phys. Rev. C* **81**, 064321 (2010).
- [73] V. Prassa, T. Nikšić, G. A. Lalazissis, and D. Vretenar, *Phys. Rev. C* **86**, 024317 (2012).
- [74] S. Quan, Z. P. Li, D. Vretenar, and J. Meng, *Phys. Rev. C* **97**, 031301(R) (2018).
- [75] Z. P. Li, T. Nikšić, and D. Vretenar, *J. Phys. G* **43**, 024005 (2016).
- [76] S. Quan, Q. Chen, Z. P. Li, T. Nikšić, and D. Vretenar, *Phys. Rev. C* **95**, 054321 (2017).
- [77] Z. P. Li, J. M. Yao, D. Vretenar, T. Nikšić, H. Chen, and J. Meng, *Phys. Rev. C* **84**, 054304 (2011).
- [78] Y. Fu, H. Mei, J. Xiang, Z. P. Li, J. M. Yao, and J. Meng, *Phys. Rev. C* **87**, 054305 (2013).
- [79] J. Xiang, Z. P. Li, W. H. Long, T. Nikšić, and D. Vretenar, *Phys. Rev. C* **98**, 054308 (2018).
- [80] J. Xiang, J. M. Yao, Y. Fu, Z. H. Wang, Z. P. Li, and W. H. Long, *Phys. Rev. C* **93**, 054324 (2016).
- [81] Z. Shi and Z. P. Li, *Phys. Rev. C* **97**, 034329 (2018).
- [82] FRIB, Facility for rare isotope beams (at Michigan State University), <https://frib.msu.edu/news/index.html>.
- [83] HIAF, The major national science and technology infrastructure project high intensity heavy-ion accelerator facility, <http://hiaf.impicas.ac.cn/hiafen/public/>.
- [84] J. Libert, M. Girod, and J.-P. Delaroche, *Phys. Rev. C* **60**, 054301 (1999).
- [85] L. Próchniak, P. Quentin, D. Samsoen, and J. Libert, *Nucl. Phys. A* **730**, 59 (2004).
- [86] P. Ring and P. Schuck, *The Nuclear Many-Body Problem* (Springer-Verlag, Heidelberg, 1980).
- [87] D. Inglis, *Phys. Rev.* **103**, 1786 (1956).
- [88] S. Beliaev, *Nucl. Phys.* **24**, 322 (1961).
- [89] M. Girod and B. Grammaticos, *Nucl. Phys. A* **330**, 40 (1979).
- [90] Y. Tian, Z. Y. Ma, and P. Ring, *Phys. Lett. B* **676**, 44 (2009).
- [91] J. Xiang, Z. P. Li, Z. X. Li, J. M. Yao, and J. Meng, *Nucl. Phys. A* **873**, 1 (2012).
- [92] NNDC, National nuclear data center, Brookhaven National Laboratory, <https://www.nndc.bnl.gov/ensdf/>; <https://www.nndc.bnl.gov/be2/>.
- [93] N. J. Stone, *At. Data Nucl. Data Tables* **90**, 75 (2005).
- [94] N. Zamfir and R. Casten, *Phys. Lett. B* **260**, 265 (1991).
- [95] E. A. McCutchan, D. Bonatsos, N. V. Zamfir, and R. F. Casten, *Phys. Rev. C* **76**, 024306 (2007).
- [96] J. Meng, J. Peng, and S. Q. Zhang, and P. W. Zhao, *Front. Phys.* **8**, 55 (2013).
- [97] S. N. T. Majola, Z. Shi, B. Y. Song, Z. P. Li, S. Q. Zhang, R. A. Bark, J. F. Sharpey-Schafer, D. G. Aschman, S. P. Bvumbi, T. D. Bucheret, D. M. Cullen, T. S. Dinoko, J. E. Easton, N. Erasmus, P. T. Greenlees, D. J. Hartley, J. Hirvonen, A. Korichi, U. Jakobsson, P. Jones *et al.*, *Phys. Rev. C* **100**, 044324 (2019).